HOLOS

Influence of heat treatment on Zr-1.0Nb-1.0Sn-0.1Fe fuel rods: Microstructure evolution, mechanical properties and fretting wear behavior

D.A. Baêta, N. Medeiros*

Escola de Engenharia Industrial e Metalúrgica de Volta Redonda - Universidade Federal Fluminense
ORCID ID: https://orcid.org/0000-0002-8686-9529*
neilmedeiros@id.uff.br*

ABSTRACT

In this work, the behavior of Zr-1Nb-1Sn-0.1Fe fuel rods was studied by subjecting them to physical tests aimed at reproducing the occurrence of fretting. For that, heat treatments were carried out on the surfaces of the fuel rods at different temperatures to modify the microstructure (α-Zr to β-Zr) and improve the mechanical properties. Mechanical tests and microstructural characterization confirmed the improvement in the mechanical properties and the modification of the alloy microstructure. The fretting tests were carried out in equipment designed to induce horizontal displacements to the fuel rods in relation to spacer grid. It was verified, through confocal microscopy, that the fretting wear mechanisms observed in the fuel rods include abrasion, adhesion, and plastic deformation, and that the increase in the heat treatment temperature decreases the mass loss, indicating a mild fretting wear regime.

KEYWORDS: Fuel rods, spacer grids, heat treatments, fretting wear, Zr-1.0Nb-1.0Sn-0.1Fe alloy

Influência de tratamentos térmicos sobre varetas combustíveis de Zr-1.0Nb-1.0Sn-0.1Fe: Evolução microestrutural, propriedades mecânicas e comportamento sob desgaste por fretting

RESUMO

Neste trabalho, estudou-se o comportamento de varetas combustíveis de Zr-1Nb-1Sn-0,1Fe submetendo-as a ensaios físicos visando reproduzir a ocorrência de fretting. Para tanto, tratamentos térmicos foram realizados nas superfícies das varetas combustíveis em diferentes temperaturas para modificar a microestrutura (α-Zr a β-Zr) e melhorar as propriedades mecânicas. Os testes mecânicos confirmaram a melhora nas propriedades mecânicas e ensaios de caracterização microestrutural evidenciaram alterações da microestrutura da liga. Os ensaios de fretting foram realizados em equipamentos projetados para induzir deslocamentos horizontais das varetas combustíveis em relação à grade espaçadora. Verificou-se, por microscopia confocal, que os mecanismos de desgaste por fretting observados nas varetas combustíveis incluem abrasão, adesão e deformação plástica, e que o aumento da temperatura de tratamento térmico diminui a perda de massa, indicando desgaste por fretting menos severo

Palavras chave: Elementos combustíveis, grades espaçadoras, tratamentos térmicos, desgaste por fretting, liga Zr-1.0Nb-1.0Sn-0.1Fe.

1. INTRODUCTION

Nuclear energy is the most efficient source among alternatives to fossil fuels, being responsible for a significant portion of electricity supply in the developed countries. Therefore, it is essential to ensure the safety of nuclear power plants, eliminating or minimizing unexpected accidents.

For years, fretting wear has been recognized as a significant deficiency in various industrial applications. Fretting wear is associated with the long-term service of operating mechanical and engineering components, including aircraft engine couplings (Leen *et al.*, 2002), locomotive axles (Zhen *et al.*, 2010), and nuclear fuel (Lee *et al.*, 2013). Hoeppner (2006) presented an overview of fretting failures in real structures. Fretting damage occurs when two contact surfaces are submitted into a relative oscillatory movement of small amplitude, which causes a reduction in component life.

One of the most common and expensive problems that presents a major safety concern in nuclear power plants is the damage caused by fretting wear due to flow-induced vibration (FIV) between the fuel rod and grid, which is the main contribution to fuel rod failure in pressurized water reactors (PWRs). This is a serious problem, as damage caused by fretting wear on the fuel rods can lead to perforation and consequent leakage of radioactive material. According to Kim (2009) and Lorenzo-Martin and co-workers (2019), more than half of the leak incidents result from grid-to-rod fretting wear damage.

The material used in nuclear fuel coatings in nuclear reactors is made of zirconium alloys, which are susceptible to fretting wear. The zirconium alloys are highly desirable due to their good mechanical behavior, corrosion resistance, and low thermal absorption cross-section of neutrons. However, wear resistance is lower than that of nickel alloys and stainless-steel nuclear materials. In the last decades, Zr alloys, such as the Zircaloy family were developed and had their resistance to fretting wear tested, as evaluated by Cho *et al.* (1998), Lin *et al.* (2016) and Qu *et al.* (2016). More recent alloys optimized to improve corrosion resistance and mechanical resistance, such as Zirlo (ZrNbSnFe), replaced the Zircaloy alloy in PWRs (Sabol 2006), Jiao *et al.* (2023), Kumara *et al.* (2022), Reed *et al.* (2021) e Fazi *et al.* (2023).

The commercial alloy Zr-1.0Nb-0.7Sn-0.1Fe has been widely used in the fabrication of fuel assembly parts as fuel rods and spacer grids. This material is very attractive in nuclear applications due to high wear and corrosion resistance and, also, good mechanical properties. These aspects were also extensively addressed by Li et al. (2021).

Guo *et al.* (2018), when performing fretting tests with an alloy 405 in as-received condition and heat-treated, demonstrated that the sample with greater hardness showed less damage by fretting.

Tang *et al.* (2014) concluded that mechanical contact behavior of the thin wall tube sample is significantly different when compared to the behavior of a standard thickness sample under the effect of the same load. Therefore, it is necessary to study the fretting behavior directly under the thin wall of the fuel rod.

Fu *et al.* (2000) showed that several approaches are used to mitigate or reduce frictional wear in nuclear plants. Among them, it can be considered design changes in some

components of fuel assemblies. This approach is not always possible and can be costly, as any change in the design must undergo rigorous testing and, frequently, recertification. Lubricating contact surfaces is another approach often considered. This approach is easy to implement, but not always effective, due to the limited role of the lubricant during wear conditions (low sliding speed and high contact pressure). Under these conditions, composition and topography of the surface of the materials in contact are more important. The third approach to wear reduction is surface engineering/phase transformation.   This approach is more promising because fretting damage is a surface-related mechanism that involves mechanical and chemical events on the surface of the material.

Park *et al.* (2019) observed a lower mass loss during fretting wear tests on heat-treated samples. In their studies, they demonstrated that the wear loss of the heat-treated sample was relatively smaller when compared to the as-received material. Therefore, the strategies that optimize the composition, such as alloy with other elements and/or manipulation of heat treatment procedures, are often adopted to improve the mechanical and corrosion properties of zirconium alloys.

Baêta *et al.* (2020) showed that the misalignment promoted premature wear because there is the intensification of fretting wear occurred by the appearance of complementary efforts that influenced the micro-superficial wear in contact regions, accelerating the phenomenon of fretting. In the same study it was possible to evaluate the material fretting wear from performed tests at cool and with dry conditions in terms of the increasing of cycles number and taken into account the misalignment effect. The results indicated that the wear mechanism was controlled by debris generation along sample-spacer grid contact surfaces.

Baêta *et al.* (2021) observed that fretting wear mechanisms in the fuel rods include abrasion, adhesion, and plastic deformation, and non-thermally treated samples showing a more severe fretting wear mechanism (abrasion).

Based on this context, in the present work the effects of heat treatment and microstructural evolution on mechanical resistance and fretting wear behavior outside the reactor of the Zr-1.0Nb-0.7Sn-0.1Fe nuclear rods were investigated. For this purpose, a mechanical apparatus was proposed to reproduce fretting wear phenomenon, which allows the analysis of the grid-to-rod fretting behavior directly in the thin wall of the fuel rod and to use a complete set of the grid. The devised prototype enables the evaluation of the superficial wear on the fuel rods from the material mechanical behavior and the fretting fatigue occurrence on fuel assembly components in dry conditions for a distinct number of cycles.

2. MATERIAL AND METHODS

2.1. Material

Tubular rods used in 16x16 type nuclear fuels with 1000mm in length and 9.13mm outside diameter, manufactured from a commercial Zr-1Nb-1Sn-0.1Fe alloy, were used to investigate the fretting wear resistance of this material. Baêta *et al.* (2020) presented alloy typical properties for this alloy. The spacer grid used in this study, was composed of 256 cells distributed in 16 horizontal lines and 16 vertical columns. It was also manufactured by drawing process from the same Zr-1Nb-1Sn-0.1Fe alloy in the dimensions of 200mm x 200mm and 60 mm in thickness. The spacer grid inner cells, where the nuclear fuel rods are positioned, have a nominal internal dimension of 12

mm in diameter with a set of two springs and four dimples that maintain nuclear fuel rods in the direction of its longitudinal axis. These supports are equally positioned and spaced radially by 90° from each other in each cell, according to Fig. 1.
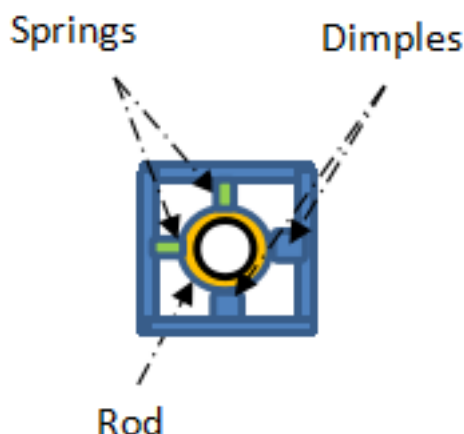

Figure 1: Schematic representation of the contact between the rod (usually filled with fuel pellets) and the springs and dimples of grid. Source: Authors (2024)

2.2. Methods

2.2.1. Heat Treatments

Thermomechanical treatments are carried out commercially to restore or improve the mechanical properties of materials during or after their manufacture. Depending on the treatment applied, different microstructures can be produced.

In order to improve the resistance to fretting wear of the Zr-1Nb-1Sn-0.1Fe alloy, fuel rod samples were vacuum encapsulated (10^{-2} bar) in quartz tubes with a 10 mm diameter. The heat treatments were carried out in a Brasimet K 250 NZ oven at 580 °C, 630 °C, 830 °C, and 960 °C for a total time of 4 hours, and then cooled in water to preserve the microstructure of high temperature.

2.2.2. Chemical Composition

X-ray fluorescence analyses were performed on the analytical diffractometer AXIO MAX PAN, in order to determine the chemical composition of the alloy under study. From the chemical composition of the alloy, the phase diagrams Zr-Nb and Zr-Sn were calculated using the commercial software ThermoCalc.

2.2.3. Microstructural Characterization

X-ray diffraction (XRD) profiles for each sample were recorded with the BRUKER D8 ADVANCED X-ray diffractometer using CuKα radiation. The 2θ ranged from 20° to 100° with a step scan of 0.02°. The time per step was 0.1 seconds.

Optical Microscopy (OM) and Scanning Electron Microscopy (SEM) were used for microstructural characterization of the material in each available condition. The rod segments were cut and had their microstructures analyzed along the longitudinal section. After sanding sequences with SiC: 220-4000, the samples were polished with 1 μm alumina and oxalic acid in a

1:4 ratio. Then, the samples were chemically etched with a 50% H_2O, 45% HNO_3, and 5% HF solution, by friction with cotton for 30 seconds.

The presence of second phase precipitates, as well as the matrix phase, were analyzed by Energy Dispersive Spectroscopy (EDS). The micrographs were obtained using the Olympus GX71 inverted microscope and the Zeiss JEOL JSM 6460LV scanning electron microscope, equipped for energy dispersive spectroscopy.

2.2.4. Mechanical Tests

Vickers microhardness tests were performed on Zr-1Nb-1Sn-0.1Fe samples in both as-received and heat-treated conditions in a Shimadzu HMV microdurometer with load of 200g and indentation time of 20 seconds.

Tensile tests on Zr-1Nb-1Sn-0.1Fe tubular samples also for as-received and heat-treated conditions were performed using an Instron 5585H universal testing machine at room temperature and for a nominal strain rate of 2.8×10^{-2} s^{-1}. These tests were performed according to ASTM E8 - Standard Test Methods for Tension Testing of Metallic Materials (2011).

2.2.5. Fretting Tests

Mechanical apparatus designed for carrying out fretting tests directly on the fuel rod and grid is shown in Figure 2. This device consists of a set of mechanical elements that produce horizontal oscillatory movement through a frequency converter. In this way, it is possible to make precise adjustments to the vertical and horizontal positions of the fuel rod, aiming at its alignment in a certain cell of the grid. The test oscillation amplitude, produced by an eccentric bearing was maintained as constant an equal to 0.07 mm.
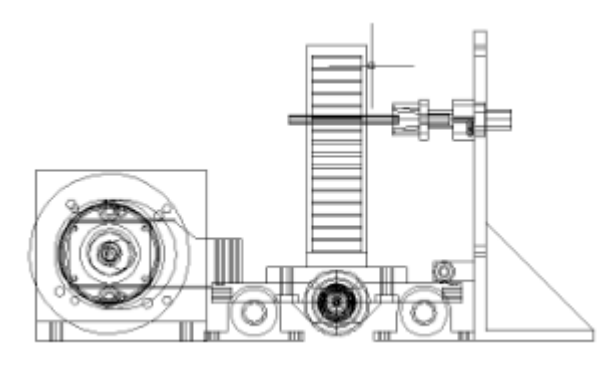

Figure 2: Grid-to-rod fretting wear test equipment. Source: Authors (2024)

Kim and Suh (2009) reported that the first signs of leakage of the nuclear fuel rods into a fuel element similar to that used in this experiment, in a wide range of operating time, were observed mainly in the periphery of the reactor core and the seven first and four last lines of the spacer grid, respectively. Thus, the nuclear fuel rod was positioned in the cell of the grid as shown in Figure 3. The fuel rod was fixed to the prototype bearing at the start of the fretting wear test, considering a constant reference distance. Fretting wear tests were carried out at room temperature and with a relative humidity of 50-60%, without lubricating fluid or presence of refrigerant. Additionally, an oscillatory movement with a frequency of 30 Hz and 106 cycles was set. After the test, the fuel rod was cleaned with acetone by ultrasound for 5 minutes and dried in compressed air to analyze the loss of material and wear out area.
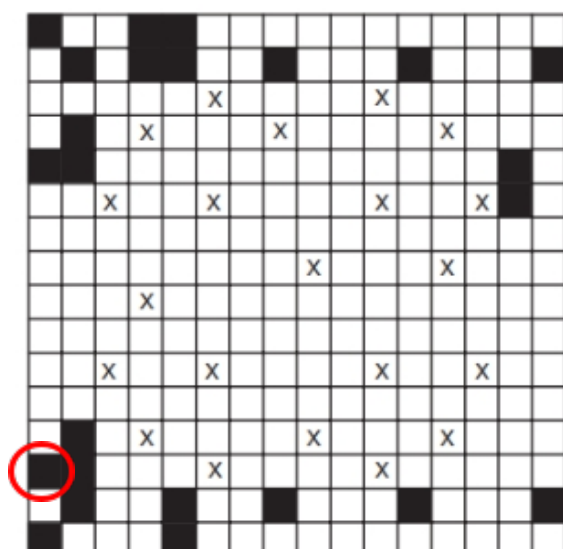
Failure of fuel rods induced by fretting wear.

X represents the positioning of the guide tubes of the fuel element set.

Positioning of the fuel rod during fretting tests.

Figura 3: Location of the failed fuel rods due to fretting wear in the 16 x 16 KOFA Fuel Element Set loaded in the Kori 2 Unit and positioning of the samples in the fretting tests. Adapted from Kim and Suh (2009).

3. RESULTS AND DISCUSSION

Table 1 shows the chemical composition (% weight) of the Zr-1Nb-1Sn-0.1Fe alloy. The results were close to typical chemical composition of this material reported by Fazi *et al.* (2023).

Table 1: Chemical composition of the Zr-1Nb-1Sn-0.1Fe alloy (% weight).

Element	(% weight)
Nb	1,03
Sn	1.0
Fe	0.11
Zr	Balance

Theoretical and experimental studies of phase stability trends in the periodic table have been an important goal of materials science and computational physics. In ambient conditions, elementary zirconium crystallizes in a hexagonal close-packed (HCP or α-phase) structure. This structure becomes body-centered cubic (BCC), commonly called β-phase, at temperatures above 600 °C. Zhang *et al.* (2005).

The reliable construction of the phase diagram is of great importance for the development of new materials and the prediction of their mechanical properties.

Figures 4 and 5 show the theoretical phase diagrams of the Zr-Sn and Zr-Nb systems, respectively. The analysis of the theoretical diagrams in the weight percentages of Sn and Nb of the alloy under study allows verification of the expected phases in the respective heat treatment temperatures.
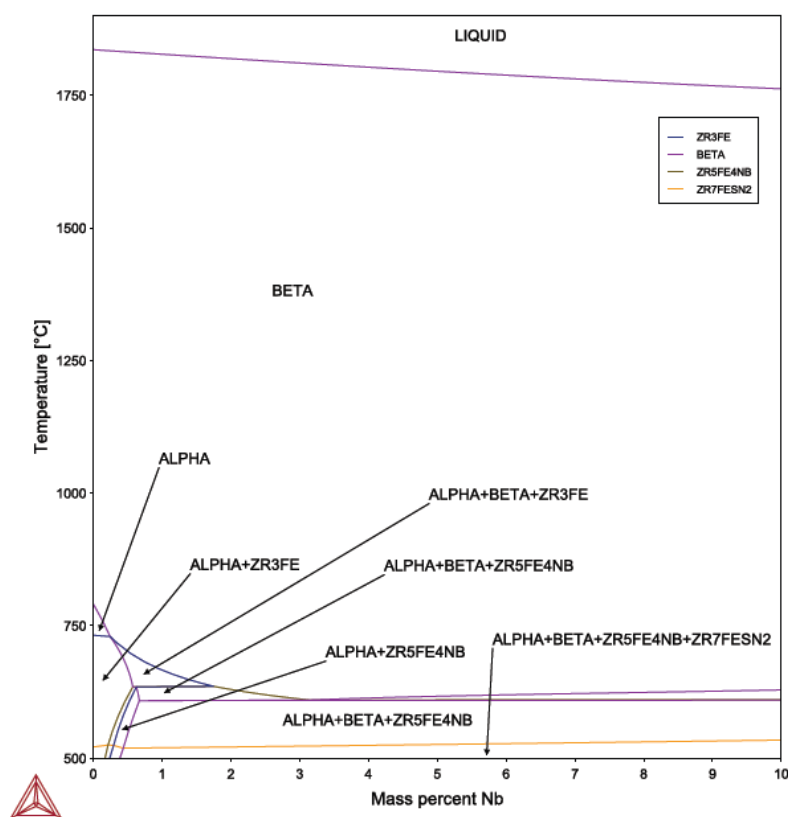
Figure 4: Theoretical diagram of the Zr-Nb system. Source: Authors (2024)
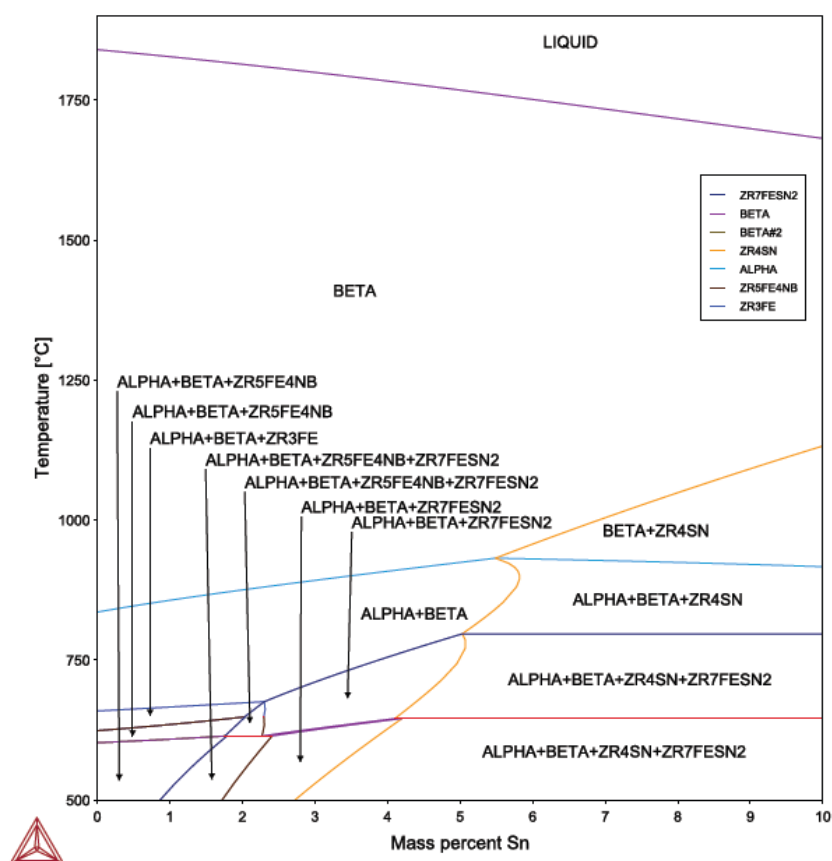

Figure 5: Theoretical diagram of the Zr-Sn system. Source: Authors (2024)

After analyzing the theoretical diagrams in the weight percentages of Sn and Nb of the alloy under study, according to Table 1, the expected phases in the heat treatment temperatures used can be inferred:

- 580°C: α-Zr, β-Nb and ZrFeNb

- 630°C: α-Zr, β-Zr and ZrFeNb

- 830°C: α-Zr and β-Zr

- 960°C: β-Zr

In the commercial ZrNb and ZrNbSnFe alloys, several phases may exist, depending on the composition of the alloy and the thermomechanical history. The commonly reported phases in these alloys are the a-Zr, b-Zr, b-Nb, and ternary ZrNbFe phases. The precipitation of the b-Nb phase and the ternary ZrNbFe phases in a-Zr are mainly due to the low terminal solid solubility (TSS) of Nb in the a-phase. Harte *et al.* (2018).

Sn, which is an a-stabilizer, reduces the solubility of Nb in the a-phase. At the Sn levels applied to commercial ZrNbSnFe alloys (Sn 1% weight), Sn and Nb coexist in solid solution. Woo e Griffiths (2009).

b-Nb can coexist with b-Zr and can be found in isolated grains or as a precipitate at the grain boundaries. Eventually, the equilibrium state is reached so that, in the case of binary phases, there are BCC b-Nb and HCP a-Zr with Nb in solid solution (<1% weight).

Northwood *et al.* (1991) reported that there is a small amount of Fe and Cr in most b particles in the Zr-2.5Nb microstructure (% by weight). Francis *et al.* (2014) reported the segregation of Fe at the b-Zr/ b-Nb interface in the ZIRLO™ with low Sn content. In both cases, it is important to consider that Fe will be segregated in the complete 3D interfacial region and, therefore, some Fe can be detected in the interfacial region above or below the precipitate.

The existence of ternary ZrNbFe intermetals has been demonstrated in quaternary ZrNbSnFe alloys, such as ZIRLO™ (Sabol, 2006) and (Francis *et al.*, 2014), NSF-2 (Kruger e Adamson, 1993) and E635 (Averin *et al.*, 2000) e (Kobylyansky *et al.*, 2008). Recent studies of ternary ZrNbFe alloys reported the existence of two dominant ternary ZrNbFe phases: the hexagonal $Zr(Nb,Fe)_2$ and the face-centered cubic $(Zr,Nb)_2Fe$. Ramos *et al.* (2007), Toffolon-Masclet *et al.* (2008) and Toffolon-Masclet *et al.* (2008).

In order to validate the obtained phase diagrams, and to verify the phases present in the samples under study, X-ray Diffraction (XRD) tests were performed. The transition between the a-Zr and b-Zr phases can be distinguished by the appearance and disappearance of their characteristic diffraction peaks, see Figure 6. The XRD patterns shows an increase of the β-phase with the increase of the heat treatment temperature. The same behavior was observed by Zhang *et al.* (2005) and Pushilina *et al.* (2015).

Kim *et al.* (2008) investigated the effect of different cooling rates on the Zr-1.5Nb-0.4Sn-0.2Fe-0.1Cr microstructure employing water quenching and air cooling. Widmanstätten structure was formed during tempering with the water at a rapid cooling rate.

The precipitates are distributed randomly within the grains and along the grain boundaries (although the grain boundaries are not very clear). The type of ZrNbFe precipitate could not be

determined since the literature reports two types of Second Phase Particles (SPPs) in Zr alloys. However, it can be inferred that the structure of SPPs is strongly dependent on the chemical composition of SPPs in the alloy. Chen *et al.* (2015) and Burr *et al.* (2013). The amount of Fe/Nb (% weight) also has a significant influence on the structure of SPPs in the alloys of the ZrNbFe system. Qiu *et al.* (2012).

In general, above 630°C, the micrographs illustrate the presence of two common characteristics in the microstructure. The first is the presence of primary α-equiaxed grains (α-Zr that did not turn into β-Zr during heating), which decrease progressively in the volume fraction with the increase of the heat treatment temperature. The second is the appearance of structures of the Widmanstätten type, which increases progressively in the volume fraction with the increase of the heat treatment temperature. Similar behavior was observed by Ahmmed *et al.* (2016) during the heat treatment of Zr-Excel alloy.

The β-Zr phase persists at room temperature due to the high cooling rate. Thus, it was possible to observe the presence of the β-phase even though it is metastable at room temperature.

Niculina *et al.* (1996) published an article in which they describe the evolution of the microstructure in the Zr±1Nb±1Sn±0.4Fe (% weight) alloys under irradiation. They suggested that the α→α+β phase transformation temperature is about 650°C, and they also precipitate $(Zr,Nb)_3Fe$, $Zr(Nb,Fe)_2$, and Zr_4Sn. Niculina *et al.* (1996) also indicated that the limit α+β→β is located at 950°C in the same alloy.
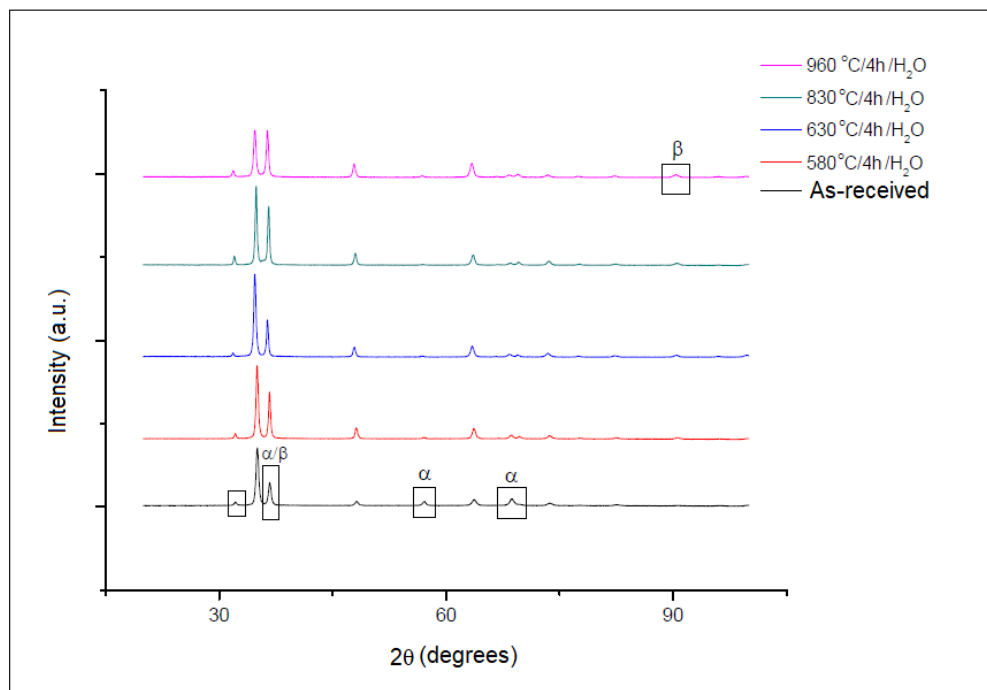

Figure 6: XRD patterns showing the phase identification between the α-Zr and β-Zr phases of the studied samples.

Source: Authors (2024)

The OM, SEM, and EDS techniques were performed to verify the characteristics of the microstructures of the samples and, when applicable, precipitates. Figures 7 to 11 show the results of these analyses. The presence of precipitates in the αZr + Zr-Nb-Fe + βNb domain is observed. In

the αZr + ZrNbFe + β-Nb domain, the precipitation of the β-Nb phase and the ternary ZrNbFe phases in α-Zr are mainly due to the low terminal solid solubility (TSS) of Nb in the α-phase. In this domain, Fe and Nb are present in the intermetallic compound, while Sn is dissolved in the α-phase. In the αZr + ZrNbFe + βZr domain, Sn is present in both αZr and βZr. In the αZr + βZr region, Fe concentration decreases during heating, while Sn and Nb levels increase in βZr.
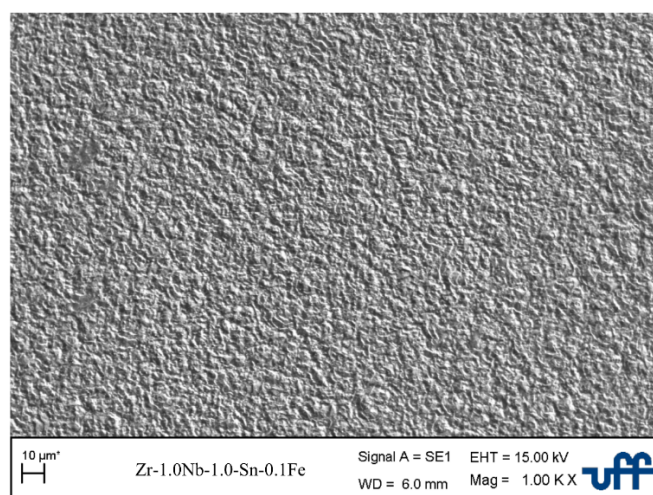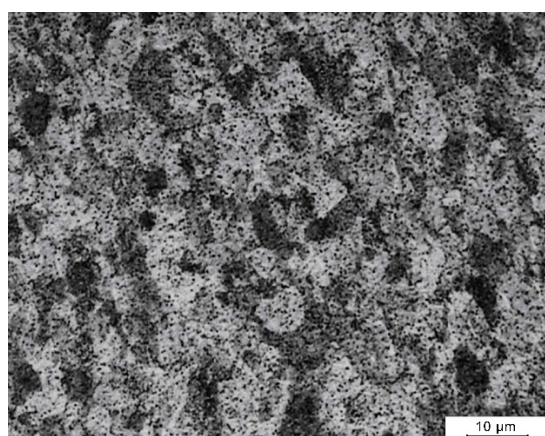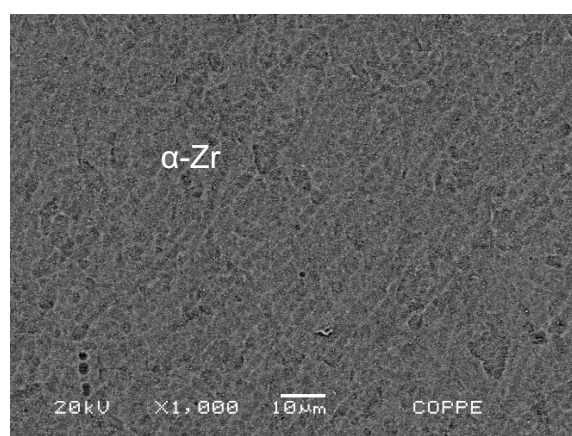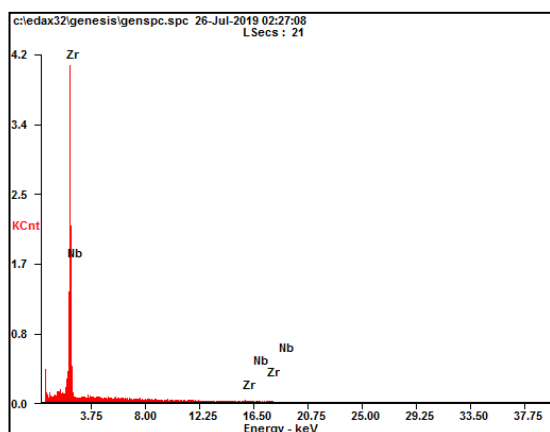

Figure 7: SEM micrograph of Zr–1.0Sn–1.0Nb–0.1Fe as-received specimen. Source: Authors (2024)
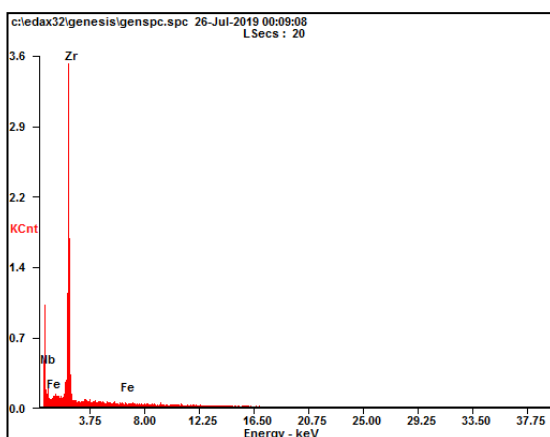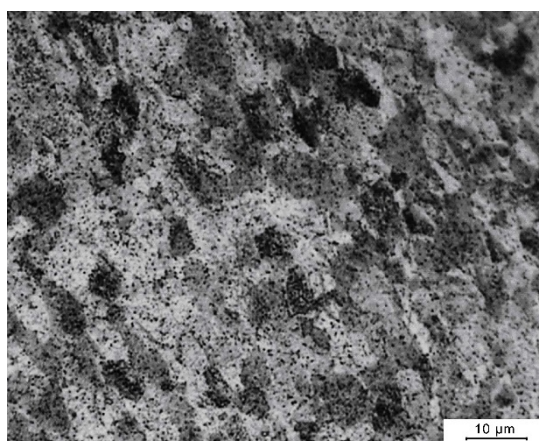

a)

b)

c)

Element	% Weight	% Atom.
Zr	87.50	87.70
Nb	12.50	12.30

d)

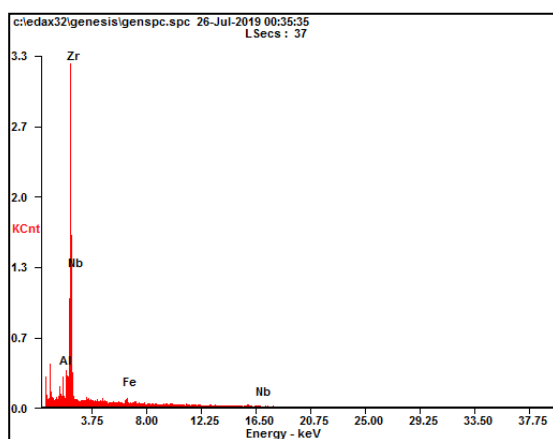| Element	% Weight	% Atom.
Zr	88.36	87.78
Nb	9.07	8.31
Fe	2.57	3.91

Figure 8: OM and SEM micrographs and EDS spectrum for Zr–1.0Sn–1.0Nb–0.1Fe specimen precipitates treated by 560°C/4 hours. Source: Authors (2024)

a)
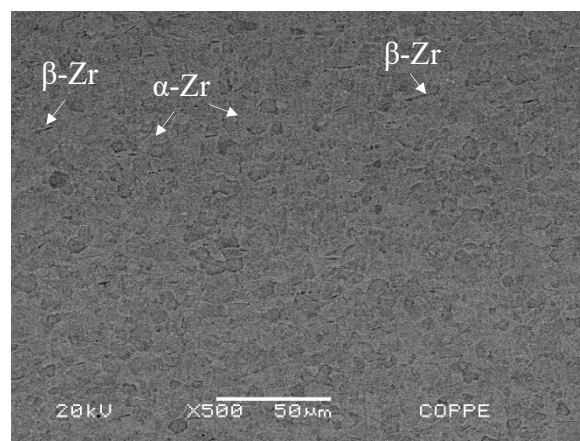
b)

Element	% Weight	% Atom.
Zr	87.20	86.38
Nb	9.69	8.88
Fe	3.11	4.74

c)

Figure 9: OM and SEM micrographs and EDS spectrum for Zr–1.0Sn–1.0Nb–0.1Fe specimen precipitates treated by 630°C/4 hours. Source: Authors (2024)
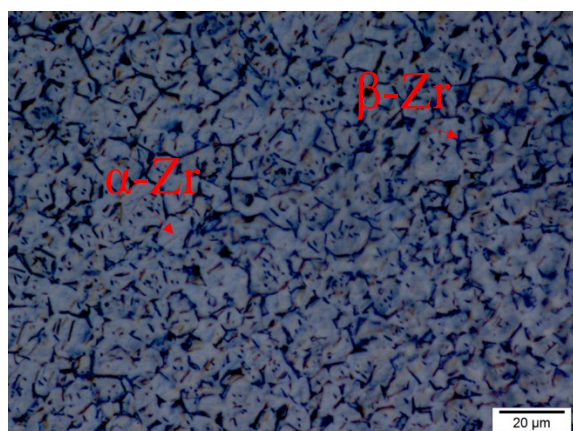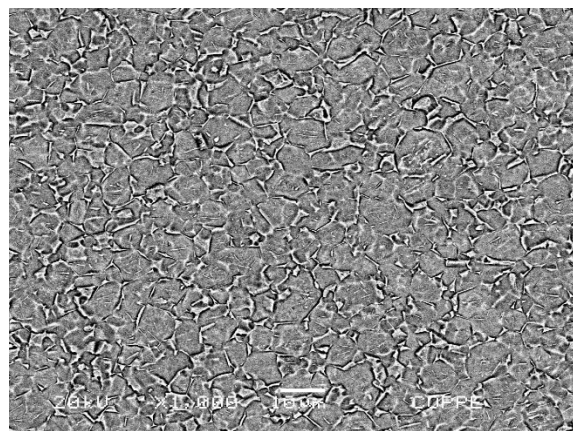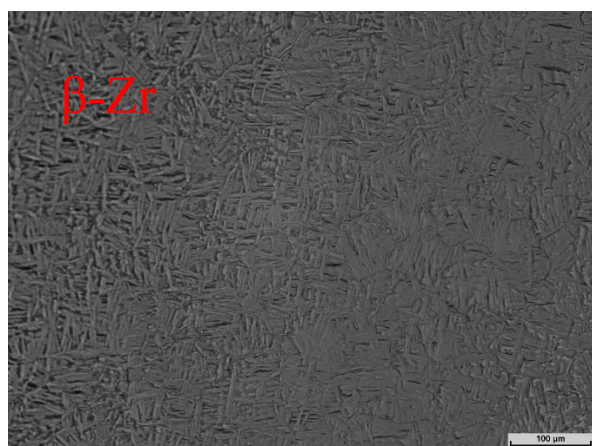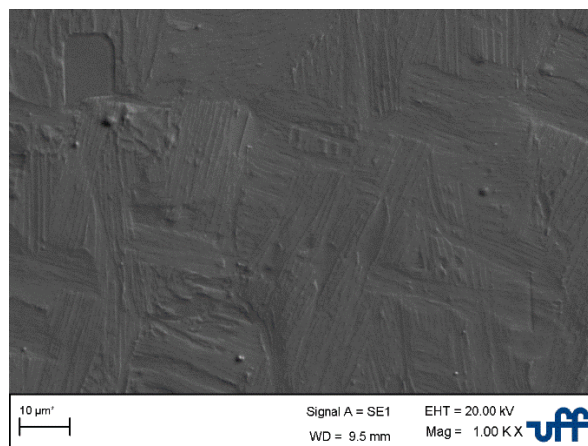

a)

b)

Figure 10: OM and SEM micrographs of Zr–1.0Sn–1.0Nb–0.1Fe specimen treated by 830°C/4 hours. Source: Authors (2024)

a)

b)

Figure 11: OM and SEM micrographs of Zr–1.0Sn–1.0Nb–0.1Fe specimen treated by 960°C/4 hours. Source: Authors (2024)

Table 2 shows the results of Vickers microhardness of the heat-treated and as-received samples. Microhardness was measured for the as-received material and compared to those obtained after each heat treatment. The hardness of the material increased from 191 ± 26.69 HV to 399 ± 18.57 µHV with the increase of the heat treatment temperature.

Table 2: Vickers microhardness results for each condition analyzed.

As-received condition = 191 ± 26.69				
Thermal treatment	580°C	630°C	830°C	960°C
Vickers Microhardness	244 ± 9.13	268 ± 10.61	396 ± 14.86	399 ± 18.57

Table 3 shows the mechanical properties of Zr-1Nb-1Sn-0.1Fe alloys at different heat treatment temperatures. It was verified that the treated samples presented values of yield limit, ($\sigma_y^{0.2\%}$), and tensile strength, (σ_{uts}), higher than the as-received samples.

Table 3: Mechanical properties of the samples

Temperature (°C)	$\sigma_y^{0.2\%}$ (MPa)	σ_{uts} (MPa)
As-received	603	754
580°C/4h	619	829
630°C/4h	624	831
830°C/4h	633	836
960°C/4h	637	882

The values obtained for Vickers microhardness and the mechanical properties of tensile strength show that these properties can change with heat treatment. The increase in Vickers microhardness values and mechanical properties in the α + ZrNbFe domain may be related to the presence of precipitates. In the α + β domain, the microstructure composed essentially of the α → β transition variant in a typical morphology of Widmanstätten may be responsible for improving mechanical properties. Chen *et al.* (2015), Yang *et al.* (2012) and Jha *et al.* (2016).

Figure 12 shows the scars on the samples after the fretting test. All fretting marks were elliptical.
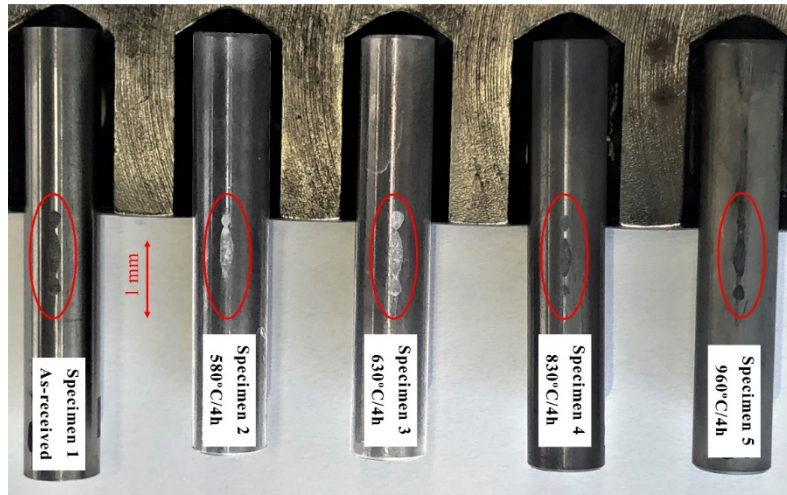
Figure 12: Fretting marks between the spring and the fuel rod after the fretting test (10^6 cycles).

Source: Authors (2024)

The heat-treated samples show less mass loss and a smaller fretting area with increasing heat treatment temperature, as shown in Table 4. It was also verified that the mass loss, as well as the fretting area, decreases with the increase of the heat treatment temperature, demonstrating that the samples treated at higher temperatures show greater fretting wear resistance, corroborating the results of increased mechanical properties of traction and Vickers microhardness.

Table 4: Mass loss values and fretting area.

Temperature (°C)	Mass loss (g)	Fretting Area (mm²)
As-Received	0.0050 ± 0.14%	14.324 ± 2.95%
580°C/4h	0.0030 ± 0.10%	12.896 ± 3.29%
630°C/4h	0.0026 ± 0.15%	11.626 ± 2.12%
830°C/4h	0.0018 ± 0.18%	7.995 ± 1.98%
960°C/4h	0.0006 ± 0.05%	6.701± 1.12%

The fretting fatigue process is usually divided into different stages. The initial phase is mostly dominated by the oxide layer on the contact surfaces. After the oxide layer is worn, cold welds are formed on the surface roughness, increasing the friction coefficient. Subsequent loading of the surfaces causes these micro welds to break, forming wear residues. These wear residues can work as an abrasive, but they can also form a third protective layer, reducing wear (Sunde *et al.*, 2018). Additional loading cycles can introduce plastic deformations and micro cracks on the surfaces. If the increasing rate of fretting wear depth is greater than the crack propagation rate, the crack will be removed along with material loss, and new initial cracks will occur in different locations due to the change in contact geometry. Tang *et al.* (2014). Thus, material removal due to surface wear can eliminate the nucleation of crack on the surface.

In order to know the characteristics of the material and the fretting wear nature of the affected area, the region was evaluated using the Scanning Electron Microscopy (SEM) technique. Figures. 13 to 17 show the SEM micrographs of the samples in the fretting areas.

The SEM images show that fretting wear occurs in some regions through the thinning out of small particles in grooves, and in other regions through the pull out of larger particles. The latter results in craters with rough surfaces, which are prevalent in the affected region.

It is observed that the treated samples have less material pull out than the untreated sample. Figures. 13 to 17 show that worn surfaces have valleys due to material pull out and that the samples treated at 830°C (Figure 16) and 960°C (Figure 17) show cracks on their surfaces. These cracks are formed due to frictional force between the spring and the rod. This force induces shear in the material, leading to a pull out of the alloy and formation of craters.
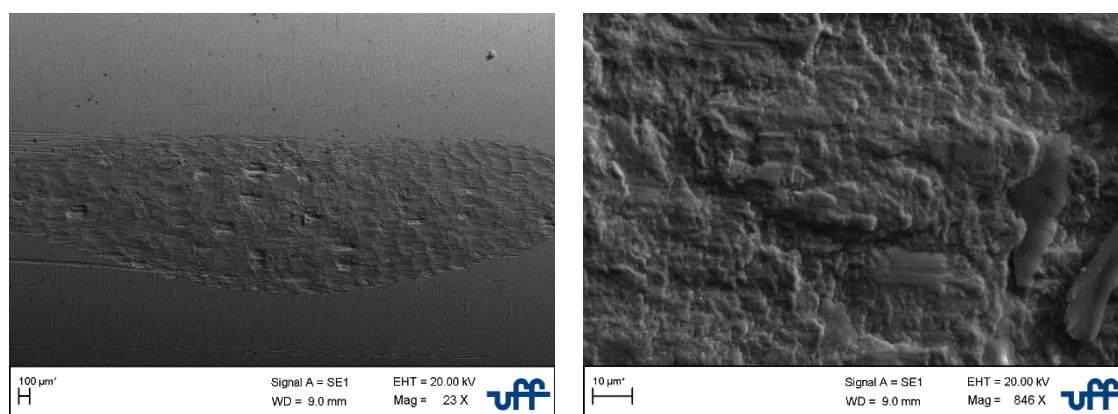

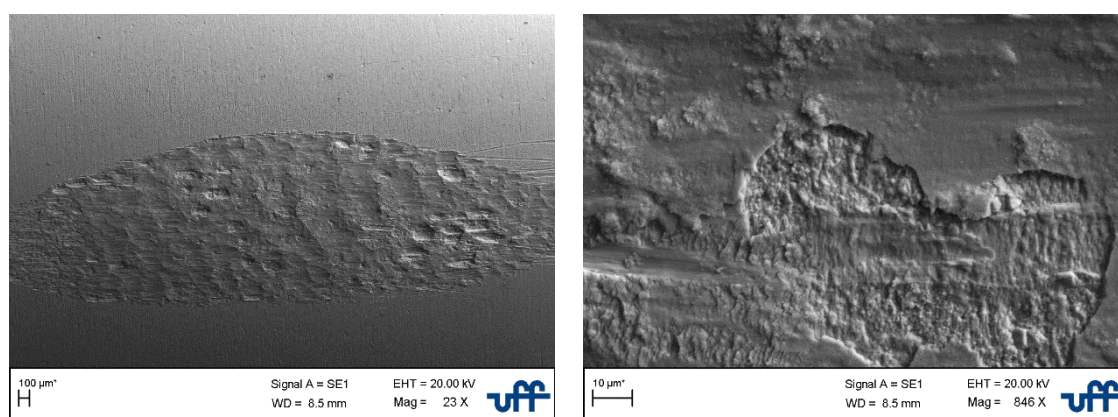**Figure 13: SEM of grid-to-rod fretting marks of the sample as-received (Specimen 1). Source: Authors (2024)**

Figure 14: SEM of grid-to-rod fretting marks of the sample treated at 580°C/4h (Specimen 2).
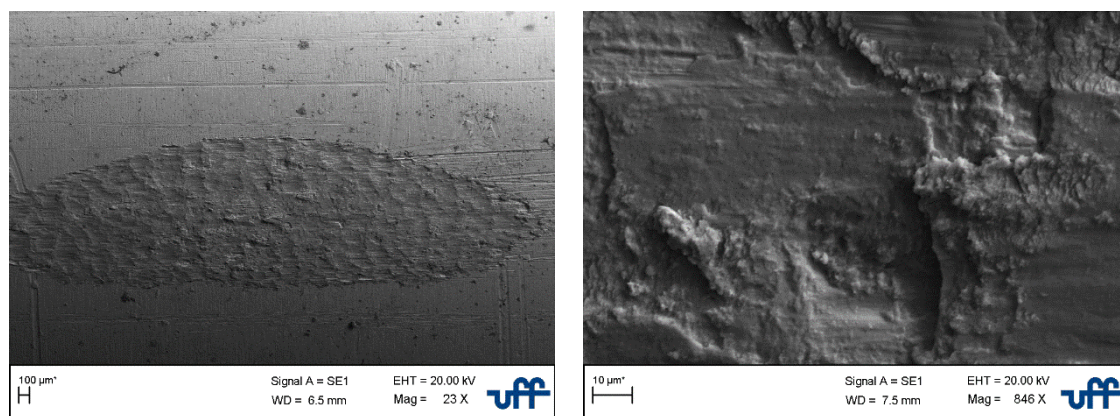
Source: Authors (2024)

Figure 15: SEM of grid-to-rod fretting marks of the sample treated at 630°C/4h (Specimen 3).
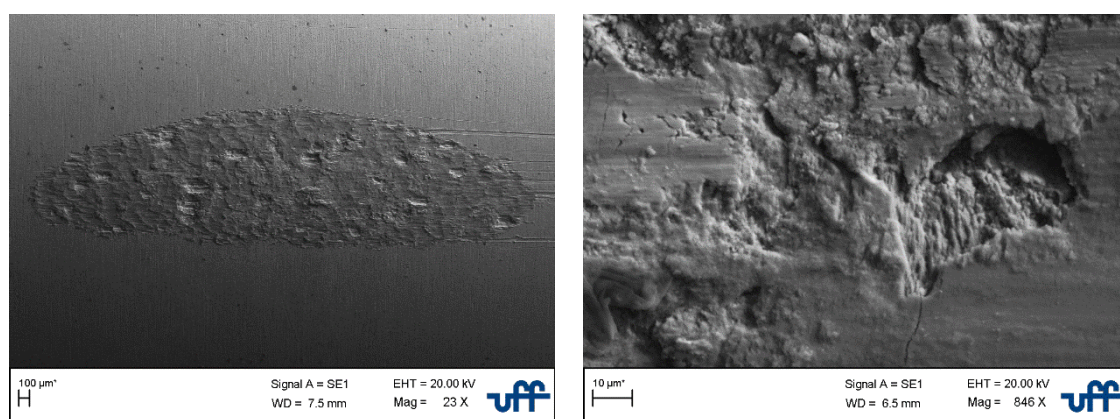
Source: Authors (2024)

Figure 16: SEM of grid-to-rod fretting marks of the sample treated at 830°C/4h (Specimen 4).

Source: Authors (2024)

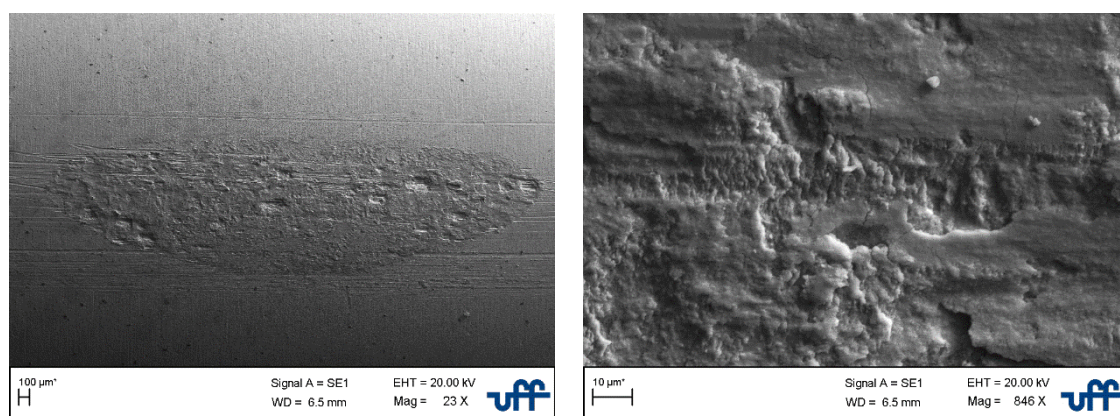**Figure 17: SEM of grid-to-rod fretting marks of the sample treated at 960ºC/4h (Specimen 5).**

Source: Authors (2024)

4. CONCLUSIONS

In this study, samples of nuclear rods made from a Zr-1.0Nb-1.0Sn-0.1Fe alloy and used in 16x16 type nuclear fuel were treated at different temperatures and subjected to characterization analyses and tests of mechanical properties and fretting. The results provided an understanding of

how the phase changes of the material influence the mechanical properties and topographic wear of the surface. These are summarized as follows:

(1) The heat treatment influenced microhardness and mechanical properties. The increase in the heat treatment temperature promoted an increase in the microhardness values and the tensile strength of the material;

(2) According to the microhardness values and the DRX profiles for each heat treatment temperature, it was possible to relate the present phase according to the phase diagrams. It was possible to observe that the increase in hardness is related to the present of precipitates and β-Zr phase in the alloy;

(3) The microscopies of samples treated with temperatures below the transition temperature show a microstructure with defined grains and the presence of precipitates. In the samples treated above the transition temperature, microscopy shows a microstructure without the presence of precipitates and Widmanstätten structures;

(4) It was possible, using the EDS technique, to observe and obtain the chemical composition of the precipitates present in the alloy, along with its matrix phase;

(5) All samples showed elliptical fretting scars. Also, the mass loss, as well as the fretting wear area, was found to decrease with the increase of the heat treatment temperature, demonstrating that there was less material pull out during the performance of the fretting tests;

(6) Finally, it was observed that worn surfaces form valleys due to material pull out and that samples treated at 830 ºC (Fig. 16) and 960 ºC (Fig. 17) show cracks on their surfaces. As for the untreated sample and samples treated at 580 ºC and 630 ºC, the presence of cracks was not observed. Thus, the removal of material due to surface wear may have been responsible for eliminating the nucleation of cracks on the surface.

AGRADECIMENTOS

5. REFERENCES

Ahmmed, K.F., Daymond, M.R., Gharghouri, M.A. (2016). Microstructural evaluation and crystallographic texture modification of heat-treated zirconium Excel pressure tube material. Journal of Alloys and Compounds, (687), 1021-1033. doi: 10.1016/j.jallcom.2016.05.072

Averin, S.A., Panchenko, V.L., Kozlov, A.V., Sinelnikov, L.P., Shishov, V.N., Nikulina, A.V., 2000. Evolution of dislocation and precipitate structure in Zr alloys under long-term irradiation. In: Zircon. Nucl. Ind. Twelfth Int. Symp, 105-121. doi: 10.1520/STP14297S

Baêta, D.A., Costa, D.J.R., Cardoso, F.G., Medeiros, N., 2020. Evaluation of fretting wear occurrence on the surface of nuclear fuel rods of Zr–1Nb–1Sn-0.1Fe alloy: Effects of assembly misalignment and grid spring loading. Wear 460–461, 203422.

Baêta, D.A., Costa, D.J.R, Medeiros, N., 2021. Analysis of heat treatment effect on fretting fatigue occurrence in Zr-1Nb-1Sn-0.1Fe fuel rods. Prog. Nucl. Ener. 140, 103923.

Burr, P.A., Murphy, S.T., Lumley, S.C., Wenman, M R., Grimes, R.W., 2013. Hydrogen solubility in zirconium intermetallic second phase particles. J. Nucl. Mater. 443, 502–506.

Chen, L., Li, J., Zhang, Y., Zhang, L.C., Lu, W., Wang, L., Zhang, L., Zhang, D., 2015. Zr–Sn–Nb–Fe–Si–O alloy for fuel cladding candidate: Processing, microstructure, corrosion resistance and tensile behavior. Corrosion Sci. 100, 332–340.

Cho, K.H., Kim, T.H., Kim, S.S., 1998. Fretting wear characteristics of Zircaloy-4 tube. Wear 219, 3–7.

Fazi, A., Sattari, M., Stiller, K., Andrén, H.O., Thuvander, M., 2023. Performance and evolution of cold spray Cr-coated optimized ZIRLO™ claddings under simulated loss-of-coolant accident conditions. J. Nucl. Mater. 576, 154268.

Felipe, E. C. B., & Ladeira, A. C. Q. (2014). ESTUDO DA SEPARAÇÃO DO PAR ZIRCÔNIO E HÁFNIO POR TROCA IÔNICA. HOLOS, 3, 291–298. https://doi.org/10.15628/holos.2014.1769

Francis, E.M., Harte, A., Frankel, P., Haigh, S.J., Jädernäs, D., Romero, J., Hallstadius, L., Preuss, M., 2014. Iron redistribution in a zirconium alloy after neutron and proton irradiation studied by energy-dispersive X-ray spectroscopy (EDX) using an aberration-corrected (scanning) transmission electron microscope. J. Nucl. Mater. 454, 387-397.

Fu, Y., Wei, J., Batchelor, A.W., 2000. Some considerations on the mitigation of fretting damage by the application of surface-modification Technologies. J. Mater. Proc. Tech. 99, 231–245.

Guo, X., Lai, P., Tang, L., Lu, J., Wang, J., Zhang, L., 2018. Fretting wear of alloy 690 tube mated with different materials in high temperature water. Wear 400-401, 119–126.

Harte, A., Griffiths, M., Preuss, M., 2018. The characterization of second phases in the Zr-Nb and Zr-Nb-Sn-Fe alloys: A critical review. J. Nucl. Mater. 505, 227-239.

Hoeppner, D.W., 2006. Fretting fatigue case studies of engineering components. Tribol. Int. 39, 1271–1276. Jha, S.K., Keskar, N., Vishnu Narayan, K.I., Mani Krishna, K V., Srivastava, D., Dey, G.K., Saibaba, N., 2016. Microstructural and textural evolution during hot deformation of dilute Zr-Sn alloy. J. Nucl. Mater. 482, 12-18.

Kim, H.G., Baek, J.H., Kim, S.D., Jeong, Y.H., 2008. Microstructure and corrosion characteristics of Zr-1.5Nb-0.4 Sn-0.2Fe-0.1Cr alloy with α β-annealing. J. Nucl. Mater. 372, 304–311.

Kim, K.T., 2009. The study on grid-to-rod fretting wear models for PWR fuel. Nucl. Eng. Des. 239, 2820–2824.

Kim, K.T., Suh, J.M., 2009. Impact of Nuclear Fuel Assembly Design on Grid-to-Rod Fretting Wear. J. Nucl. Sci.Tech. 46, 149-157.

Kobylyansky, G.P., Novoselov, A.E., Ostrovsky, Z.E., Obukhov, A.V., Shishin, V.Y., Shishov, V.N., Nikulina, A.V., Peregud, M.M., Mahmood, S.T., White, D.W., Lin, Y.P., Dubecky, M.,2008. Irradiation-induced growth and microstructure of recrystallized, cold worked and quenched Zircaloy-2, NSF, and E635 alloys. J. ASTM Int. 5, 564-582.

Kruger, R.M., Adamson, R.B., 1993. Precipitate behaviour in zirconium-based alloys in BWRs. J. Nucl. Mater. 205, 242-250.

Kumara, C., Wang, R., Lu, R.Y., Deck, C., Gazza, J., Qu, J., 2022. Grid-to-rod fretting wear study of SiC/SiC composite accident-tolerant fuel claddings using an autoclave fretting bench test. Wear 488-489, 204172.

Lee, Y.H., Kim, H.K., 2013. Fretting wear behavior of a nuclear fuel rod under a simulated primary coolant condition. Wear 301, 569–574.

Leen, S., Hyde, T., Ratsimba, C., Williams, E., McColl, I., 2002. An investigation of the fatigue and fretting performance of a representative aero-engine spline coupling. J. Strain Anal. Eng. Des. 37, 565–83. Lin, Y.W., Cai, Z.B., Chen, Z.G., Qian, H., Tang, L.C., Xie, Y.C., Zhu, M.H., 2016. Influence of diameter–thickness ratio on alloy Zr-4 tube under low-energy impact fretting wear. Mater. Today Commun. 8, 79–90.

Li, Y., Liu, Y., Li, G., Dong, X., Wang, Y., Gu, Z., Zhang, Y., 2021. Iodine-induced stress corrosion cracking behavior of alloy ZIRLO with Zr coatings by electrodepositing with different pulse current densities. Corr. Sci. 193, 109890.

Lorenzo-Martin, C., Ajayi, O.O., Hartman, K., Bhattacharya, S., Yacout, A., 2019. Effect of Al2O3 coating on fretting wear performance of Zr alloy. Wear 426-427, 219-227.

Morghi, Y., Mesquita, A. Z., Puente Angulo, J. A., & Baliza Maia, A. R. (2018). SIMULAÇÃO DO ESCOAMENTO EM CONTRACORRENTE ÁGUA/AR EM REATORES NUCLEARES PWR UTILIZANDO CÓDIGO OPENFOAM. HOLOS, 6, 92–102. https://doi.org/10.15628/holos.2018.5643

Niculina, A.V., Markelov, V.A., Peregud, M.M., Voevodin, V.N., Panchenko, V.L., Kobylyansky, G.P., 1996. Phase transition temperature in the Zr-1Nb-1Sn-0.4Fe alloy. J. Nucl. Mater. 238, 205.

Northwood, D.O., Meng-Burany, X., Warr, B.D., 1991. Microstructure of Zr-2.5Nb alloy pressure tubing. In: Zircon. Nucl. Ind. 12th Symp, 156-176.

Park, C., Kim, J., Sim, A., Sohn, H., Jang, H., Chun, E.J., 2019. Influence of diode laser heat treatment and wear conditions on the fretting wear behavior of a mold steel. Wear 434-435, 202961.

Pusilina, N.S., Kudiiarov, V.N., Lider, A.M., Teresov, A.D., 2015. Influence of surface structure on hydrogen interaction with Zr–1Nb alloy. J. Alloys Comp. 645, 476-479.

Qiu, R., Luan, B., Chai, L., Zhou, Y., Chen, J., 2012. Review of second phase particles on zirconium alloys (II): Zr–Sn–Nb–Fe alloys. Chin. J. Nonf. Met. 6, 1606–1615.

Qu, J., Cooley, K.M., Shaw, A.H., Lu, R.Y., Blau, P., 2016. Assessment of wear coefficients of nuclear zirconium claddings without and with pre-oxidation. Wear 356–357, 17–22.

Ramos, C., Saragovi, C., Granovsky, M.S., 2007. Some new experimental results on the Zr-Nb-Fe system. J. Nucl. Mater. 366, 198-205.

Reed, B., Wang, R., Lu, R.Y., Qu, J., 2021. Autoclave grid-to-rod fretting wear evaluation of a candidate cladding coating for accident-tolerant fuel. Wear 466-467, 203578.

Sabol, G.P., 2006. ZIRLO: An alloy development success. In: Proceedings of the 14th International Symposium on Zirconium in Nuclear Industry. ASTM STP 1467, 3–24.

Sunde, S.L., Berto, F., Haugen, B., 2018. Predicting fretting fatigue in engineering design. Int. J. Fatigue 117, 314-326.

Tang, L., Ding, S., Qian, H., Xie, Y., Huo, Y, 2014. Fretting fatigue tests and crack initiation analysis on zircaloy tube specimens. International Journal of Fatigue 63, 154-161.

Toffolon-Masclet, C., Brachet, J.C., Servant, C., Joubert, J.M., Barberis, P., Dupin, N., Zeller, P., Limback, M., Kammenzind, B., Dean, S.W., 2008. Contribution of termo-dynamic calculations to metallurgical studies of multi-component zirconium based alloys. J. ASTM Int. 5, 101-122.

Toffolon-Masclet, C., Guilbert, T., Brachet, J.C., 2008. Study of secondary intermetallic phase precipitation/dissolution in Zr alloys by high temperature-high sensitivity calorimetry. J. Nucl. Mater. 372, 367-378.

Woo, O.T., Griffiths, M., 2009. The role of Fe on the solubility of Nb in a-Zr. J. Nucl. Mater. 384, 77-80.

Yang, Z.N., Liu, F.C., Zhang, F.C., Yan, Z.G., Xiao, Y.Y., 2012. Microstructural Evolution and mechanical properties in Zr705 during the rolling process. Mater. Sci. Eng. A. 544, 54–58.

Zhang, J., Zhao, Y., Pantea, C., Qian, J., Daemen, L.L., Rigg, P.A., Hixson, R.S., Greeff, C.W., Gray III, G.T., Yang, Y., Wang, L., Wang, Y., Uchida, T., 2005. Experimental constraints on the phase diagram of elemental zirconium. J. Phys. Chem. Sol. 66, 1213-1219.

Zheng, J.F., Luo, J., Mo, J.L., Peng, J.F., Jin, X.S., Zhu, M.H., 2010. Fretting wear behaviors of a railway axle steel. Tribol. Int. 43, 906–11.

COMO CITAR ESTE ARTIGO

SOBRE OS AUTORES
DANIELE DE AZEVEDO BAÊTA
Universidade Federal Fluminense. Possui graduação em Engenharia Química pela Universidade Federal Rural do Rio de Janeiro (2005), mestrado em Engenharia Química pela Universidade Federal Rural do Rio de Janeiro (2007) e doutorado pela Universidade Federal Fluminense (2020). Atualmente é tecnologista da Comissão Nacional de Energia Nuclear e tecnologista da Comissão Nacional de Energia Nuclear. Tem experiência na área de Engenharia Química, com ênfase em Engenharia Química, atuando principalmente nos seguintes temas: reciclagem, polímeros, agente compatibilizante, compósitos e mechanical properties.
E-mail: danbaeta@hotmail.com
ORCID-ID: https://orcid.org/0000-0003-4649-6200

NEIL MEDEIROS
Doutor em Engenharia Metalúrgica pela Universidade Federal Fluminense (2008) com estágio Pós-Doutoral na Universidade Federal Fluminense (2008-2009). Atualmente é Professor Associado do Departamento de Engenharia Mecânica da Escola de Engenharia Industrial Metalúrgica de Volta

Redonda - Universidade Federal Fluminense (EEIMVR/UFF) e Professor Credenciado junto ao Programa de Pós-graduação em Engenharia Metalúrgica (PPGEM) da EEIMVR/UFF.
E-mail: neilmedeiros@id.uff.br
ORCID-ID: https://orcid.org/0000-0002-8686-9529